

The 2015 hard-state only outburst of GS 1354–64^{*}

H. Stiele¹†, A. K. H. Kong¹

¹National Tsing Hua University, Department of Physics and Institute of Astronomy, No. 101 Sect. 2 Kuang-Fu Road, 30013, Hsinchu, Taiwan

Accepted 2016 April 13. Received 2016 April 13; in original form 2016 February 3

ABSTRACT

Since its outburst in 1997 GS 1354–64 stayed in quiescence. In June 2015 renewed activity of GS 1354–64 was observed. Based on our analysis of energy spectra and timing properties obtained from *Swift*/XRT monitoring data we found that GS 1354–64 stayed in the hard state during the entire outburst. Such a hard state only (or “failed” outburst) has also been observed in 1997. In addition, we analysed an *XMM-Newton* observation taken on August 6th. We compared variability on long and short time scales using covariance ratio and found that the ratio showed a decrease towards lower energies instead of the increase that has been found in other black hole X-ray binaries. There are now two sources (H 1743-322 and GS 1354–64) that do not show an increase towards lower energies in their covariance ratio. Both sources have been observed during “failed” outbursts and showed photon indices much harder than what is usually observed in black hole X-ray binaries.

Key words: X-rays: binaries – X-rays: individual: GS 1354–64 – binaries: close – black hole physics

1 INTRODUCTION

GS 1354–64, located at a distance of 25 – 61 kpc (Casares et al. 2009), was discovered by the all sky monitor onboard the *Ginga* satellite (Swinbanks 1987) during an outburst in 1987 (Makino 1987). During this outburst GS 1354–64 showed spectra dominated by thermal emission from an accretion disc with a power law tail at energies above 10 keV. This kind of spectra is typically observed during the high-soft state (HSS) of a black hole X-ray binary (BHB). There are two other transient sources – Cen X-2 (Francey 1971) and MX 1353-64 (Markert et al. 1979) – which have been discovered earlier and which positions are consistent with the one of GS 1354–64. Cen X-2 is one of the brightest X-ray transients and was also observed during HSS (Tanaka & Lewin 1995), while MX 1353-64 was observed during low-hard state (LHS) when the spectrum is dominated by non-thermal emission of a hot Comptonizing plasma. In case these three sources are the same source, it would show different spectral states during an outburst like most known BHBs do. Another outburst of GS 1354–64 has been detected by RXTE in 1997. During this outburst GS 1354–64 was about a factor 3 fainter than during the 1987 outburst (Revnivtsev et al. 2000). Analysis of RXTE spectra and power density spectra showed that GS 1354–64 stayed in the LHS during the entire outburst (Revnivtsev et al. 2000; Brocksopp et al. 2001).

GS 1354–64 showed another outburst between June and September 2015 that was followed by *Swift*/XRT observations

(Miller et al. 2015). During its 2015 outburst GS 1354–64 reached about the same brightness as during the 1997 outburst. The spectral and timing analysis presented in this paper showed that GS 1354–64 stayed in the LHS during the entire outburst.

2 OBSERVATIONS AND DATA ANALYSIS

In this paper, we present a comprehensive study of the spectral and temporal variability properties of GS 1354–64 observed during its 2015 outburst. Renewed activity of the source was detected in the *Swift*/BAT and MAXI monitoring observations.

2.1 *Swift*

A series of *Swift*/XRT observations have been taken to trace the outburst evolution. Here we analysed all *Swift*/XRT observations of GS 1354–64 taken in windowed timing mode between June 10th and September 20th. We extracted energy spectra of each observation using the online data analysis tools provided by the Leicester *Swift* data centre¹, including single pixel events only. In addition, we extracted power density spectra (PDS) in the 0.3 – 10 keV energy band, following the procedure outlined in Belloni et al. (2006). We subtracted the contribution due to Poissonian noise (Zhang et al. 1995), normalised the PDS according to Leahy et al. (1983) and converted to square fractional rms (Belloni & Hasinger 1990). The PDS were fitted with models composed of

^{*} Based on observations obtained with *XMM-Newton*, an ESA science mission with instruments and contributions directly funded by ESA Member States and NASA.

† E-mail: hstiele@mx.nthu.edu.tw

¹ http://www.swift.ac.uk/user_objects/

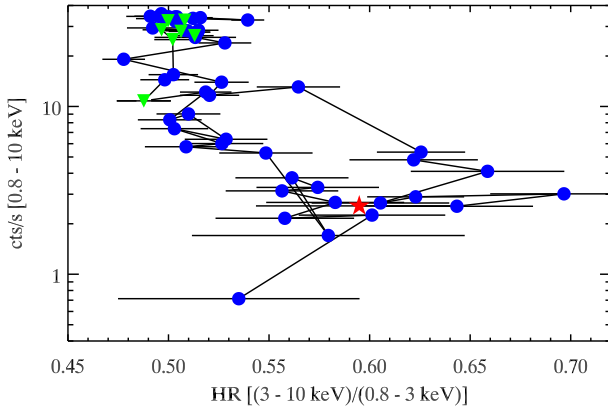


Figure 1. Hardness-intensity diagram, derived using *Swift*/XRT count rates. Each data point represents one observation. Observations in which a type-C QPO has been detected are marked by (green) triangles, and the (red) star indicates the first observation.

zero-centered Lorentzians for band-limited noise (BLN) components, and Lorentzians for quasi-periodic oscillations (QPOs).

2.2 XMM-Newton

An *XMM-Newton* ToO observation of GS 1354–64 was taken on August 6th 2015 (Obs. id.: 0727961501) with the EPIC/pn camera in timing mode. The exposure was 11.1 ks. We filtered and extracted the pn event file, using standard SAS (version 14.0.0) tools, paying particular attention to extract the list of photons not randomized in time. After using the SAS task `epatplot` to investigate whether the observation is affected by pile-up, we selected source photons from two stripes ($30 \leq \text{RAWX} \leq 35$ and $39 \leq \text{RAWX} \leq 44$) centred on the column with the highest count rate to minimize the effect of pile-up. This selection results in an observed pattern distribution that follows the theoretical prediction quite nicely. We selected single and double events (`PATTERN` ≤ 4) for our study.

We produced PDS in different energy bands for the whole observation. As for the *Swift* data, the contribution due to Poissonian noise was subtracted and the normalised PDS were converted to square fractional rms.

3 RESULTS

3.1 Swift data

3.1.1 Spectral properties

Using the *Swift*/XRT data we determined the source count rates in the total (0.8 – 10 keV), soft (0.8 – 3 keV), and hard (3 – 10 keV) energy band, and derived a hardness ratio by dividing the count rate observed in the hard band by the one obtained in the soft band. The HID of the 2015 outburst of GS 1354–64 is shown in Fig. 1 and the light curve in Fig. 2. After the detection of the outburst the source shows an increase in count rate and the HR softens. This is the “classical” behaviour of a BHB observed at the beginning of an outburst. After about 23 days the HR falls below 0.54. In the then following 18 days the count rate increases until the maximum count rate is reached on day 41; then follows a decrease in count rate. During all this time the HR stays around 0.5 (0.47 – 0.54). After day 94 the HR starts to harden. This shows that GS 1354–64

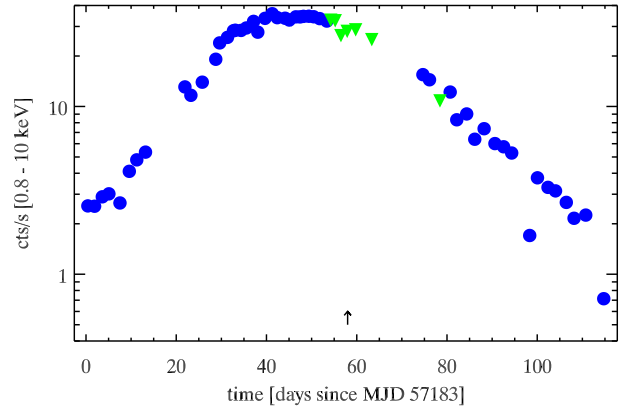
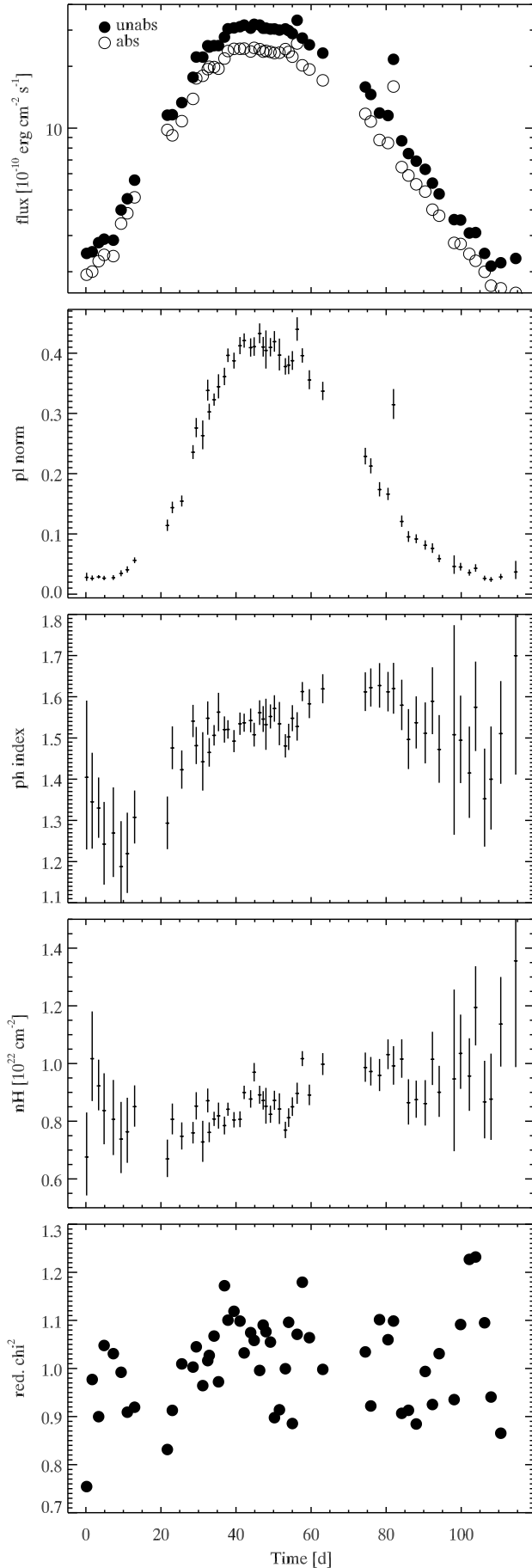


Figure 2. Light curve of the 2015 outburst, based on *Swift*/XRT count rates. Each data point represents one observation. Observations in which a type-C QPO has been detected are marked by (green) triangles. The arrow marks the date of the *XMM-Newton* ToO observation. T=0 corresponds to June 10th 2015 00:00:00.000 UTC.

remains in the hard state during its entire outburst never making it into the soft state. This type of outburst, which is a. k. a. “failed” outburst, has also been observed in the previous (1997) outburst of GS 1354–64, and in other sources like H 1743–322 (Capitanio et al. 2009; Stiele & Yu 2016), XTE 1550–564 (Sturmer & Shrader 2005), Aql X–1 (Rodríguez et al. 2006), Swift J174510.8–262411 (Del Santo et al. 2015), and V404 Cyg, A 1542–62, 4U 1543–475, GRO J0422+32, GRO J1719–24, GRS 1737–21 (Brocksopp et al. 2004).

We used XSPEC (V. 12.8.2; Arnaud 1996) to fit the energy spectra in the 0.8 – 10 keV range. Softer energies (below 0.8 keV) are omitted as the spectra are affected by a turn-up in this energy range, which is due to RMF redistribution modelling issues². Spectra were grouped to contain at least 20 counts in each bin. Grouping data allows us to use χ^2 minimisation to obtain the best fit. The observed spectra can be well described by an absorbed (`tbabs`; Wilms et al. 2000) power law model. Individual spectral parameters, using the abundances of Wilms et al. (2000) and the cross sections given in Verner et al. (1996), and reduced χ^2 values are given in Table 3. The temporal evolution of the foreground absorption, photon index, and power law normalisation are shown in Fig. 3. While the photon index shows an increase followed by a decrease during the outburst, it remains hard during the whole outburst. At the beginning of the outburst photon indices in the range of 1.3 – 1.4 are observed, while at the end photon indices are in the range of 1.4 – 1.5. Photon indices below 1.6 are unusually low for a BHB. The highest photon indices of about 1.6 are observed during outburst decay about 30 – 35 days after the maximum luminosity has been reached. The obtained photon indices depend on the observed foreground absorption as both parameters are correlated (e. g. a higher foreground absorption will lead to a smaller photon index). Using the averaged foreground absorption of $n_H = 8.6 \times 10^{21} \text{ cm}^{-2}$, the highest photon indices are reached during outburst rise, about 6 – 12 days before the maximum luminosity has been reached, and during the remaining outburst the photon indices decrease slowly. Although the evolution of the photon index depends on the assumed foreground absorption (variable versus constant), the range of observed photon indices is the same in both cases.

² http://www.swift.ac.uk/analysis/xrt/digest_cal.php

**Figure 3.** Evolution of spectral parameters.**Table 1.** Parameters of the PDS in the *XMM-Newton* observation

| Parameter | 1 – 2 keV | 2 – 10 keV |
|----------------------------|---|---|
| rms _{BLN} [%] | 14.3 ^{+0.8} _{-0.9} | 16.5 ± 0.7 |
| ν_{BLN} [Hz] | 2.85 ^{+0.85} _{-0.66} | 3.20 ^{+0.58} _{-0.52} |
| ν_{QPO} [Hz] | 0.191 ± 0.002 | 0.190 ^{+0.001} _{-0.002} |
| Δ_{QPO} [Hz] | 0.022 ± 0.004 | 0.016 ± 0.003 |
| rms _{QPO} [%] | 11.8 ^{+0.8} _{-0.9} | 13.9 ± 0.8 |
| ν_{PN1} [Hz] | 0.43 ^{+0.01} _{-0.02} | 0.40 ± 0.02 |
| Δ_{PN1} [Hz] | 0.18 ^{+0.03} _{-0.02} | 0.26 ± 0.03 |
| rms _{PN1} [%] | 13.7 ^{+0.9} _{-1.0} | 18.2 ^{+1.0} _{-1.1} |
| ν_{PN2} [Hz] | 0.074 ^{+0.007} _{-0.006} | 0.082 ^{+0.006} _{-0.005} |
| Δ_{PN2} [Hz] | 0.084 ^{+0.017} _{-0.013} | 0.077 ^{+0.013} _{-0.010} |
| rms _{PN2} [%] | 15.5 ^{+1.2} _{-0.9} | 17.5 ^{+1.2} _{-0.9} |

From spectral fits of RXTE data of the 1997 outburst of GS 1354–64 a photon index of about 1.4 to 1.5 has been obtained (Revnivtsev et al. 2000). The hard photon index indicates that the source remained in the hard state during the entire outburst. Using the obtained spectral parameters we converted the highest observed *Swift*/XRT count rate into an RXTE/PCA count rate using PIMMS. Comparing the count rate to the ones presented in Brocksopp et al. (2001) for the 1997 outburst, we found that a similar maximum brightness was reached in both outbursts. The evolution of the (un-)absorbed flux during the 2015 outburst obtained from the spectral fits is shown in Fig. 3.

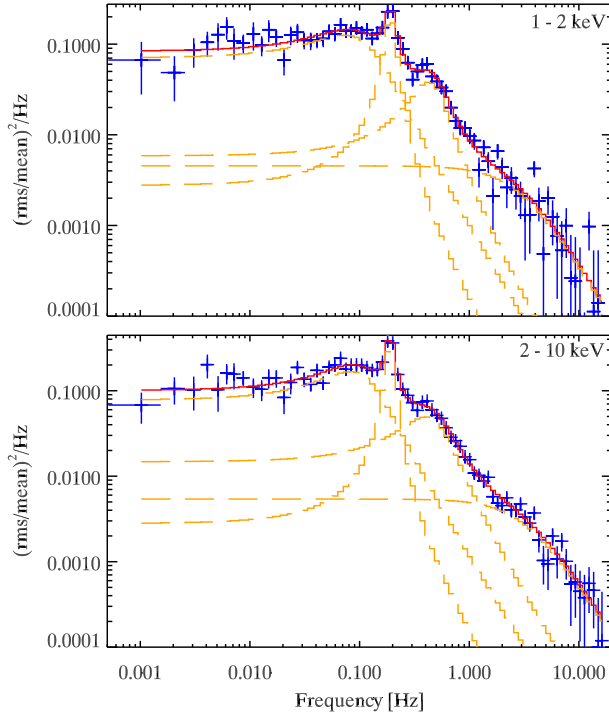
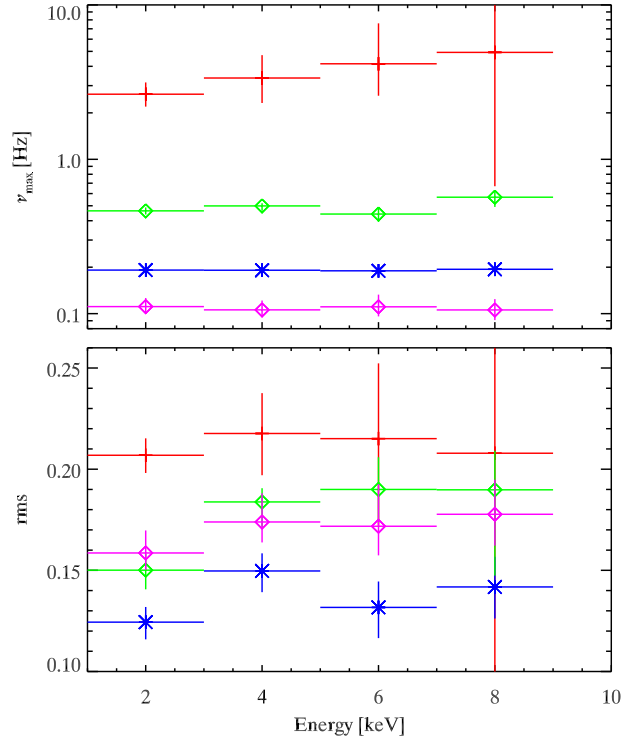
3.1.2 Timing properties

In general the PDS show a BLN component. For observations taken during outburst rise a peaked noise component with a characteristic frequency ($\nu_{\text{max}} = \sqrt{\nu^2 + \Delta^2}$, where ν is the centroid frequency, and Δ is the half width at half maximum Belloni et al. 2002) in the range of 0.03 – 0.15 Hz is present. The overall evolution of the characteristic frequency of this feature is an increase with ongoing outburst. During the entire outburst the observed fractional rms was higher than 10 per cent, which confirms that the source stayed in the hard state, as the transition to the soft intermediate state happens at fractional rms below 10 per cent (Muñoz-Darias et al. 2011). For observations taken on day 54, 55, 56, 58, 60, 63, and 78 of the outburst a type-C QPO (Wijnands et al. 1999; Casella et al. 2005) is present (parameters can be found in Table 4). All these observations are taken after the outburst reached its maximum (Fig. 2). The characteristic frequency of the QPO is in the range of 0.17 – 0.25 Hz, and the highest frequency is observed in the observation that shows the first peak in the light curve after the outburst maximum. The obtained Q values ($Q = \nu/(2\Delta)$) of these QPOs are ≥ 4.5 . For the observations taken on day 55 and 58 an upper harmonic (day 55: $Q_{\text{uh}}=5.4$, $\nu_{\text{max;uh}} = 0.42 \pm 0.02$ Hz; $\nu_{\text{max;qpo}} = 0.18 \pm 0.01$ Hz; day 58: $Q_{\text{uh}} > 47.5$, $\nu_{\text{max;uh}} = 0.399^{+0.002}_{-0.001}$ Hz; $\nu_{\text{max;qpo}} = 0.193^{+0.006}_{-0.007}$ Hz) is present, while the observation taken on day 63 shows a lower harmonic ($Q_{\text{lh}}=5.2$, $\nu_{\text{max;lh}} = 0.087^{+0.005}_{-0.006}$ Hz; $\nu_{\text{max;qpo}} = 0.195 \pm 0.007$ Hz).

Table 2. Spectral parameters obtained by fitting the EPIC/pn spectrum.

| component | model A | model B | model C | model D |
|---|---------------------------|------------------------|------------------------|-------------------------|
| N_{H} [10^{21} cm^{-2}] | $8.36^{+0.05}_{-0.04}$ | 6.76 ± 0.07 | $7.04^{+0.07}_{-0.05}$ | $8.77^{+0.20}_{-0.19}$ |
| R_{in} [km/ $\sqrt{\cos(\theta)}$] [‡] | | $55.6^{+5.2}_{-3.6}$ | $55.1^{+5.6}_{-3.7}$ | $105.3^{+19.4}_{-30.5}$ |
| T_{in} [keV] | | $0.62^{+0.03}_{-0.04}$ | $0.50^{+0.01}_{-0.02}$ | 0.33 ± 0.02 |
| Γ | $1.577^{+0.004}_{-0.003}$ | $1.44^{+0.06}_{-0.05}$ | $1.51^{+0.05}_{-0.03}$ | 1.52 ± 0.01 |
| kT_{e} [keV] | | 2.4 ± 0.1 | $10.2^{+5.0}_{-3.7}$ | |
| N_{compton} | 0.602 ± 0.003 | $0.10^{+0.03}_{-0.01}$ | 0.40 ± 0.01 | $0.41^{+0.01}_{-0.03}$ |
| rel. reflection | | $0.64^{+0.18}_{-0.15}$ | | $0.39^{+0.07}_{-0.04}$ |
| E_{cutoff} | | | 6.82 ± 0.08 | |
| E_{fold} | | | 9.4 ± 0.5 | |
| a | | | | $-0.998 - -0.930$ |
| $\log \xi$ | | | | $3.30^{+0.02}_{-0.04}$ |
| Z_{Fe} [$Z_{\text{Fe},\odot}$] | | | | 5.0 ± 0.5 |
| χ^2/dof | 2219.0/1701 | 1682.1/1697 | 1638.4/1696 | 1595.7/1695 |

Notes:

[‡]: assuming a distance of 25 kpc (Casares et al. 2009)model A: TBabs \times powerlawmodel B: TBabs \times (diskbb + reflect(nthcomp))model C: TBabs \times (diskbb + higecut \times nthcomp)model D: TBabs \times (diskbb + relxill)**Figure 4.** Power density spectra in the 1 – 2 (upper panel) and 2 – 10 keV range (lower panel) fitted with Lorentzians.**Figure 5.** Energy dependence of the characteristic frequency (upper panel) and rms spectra of the BLN (red cross), QPO (blue X), upper peaked noise (green circle), and lower peaked noise (magenta diamond).

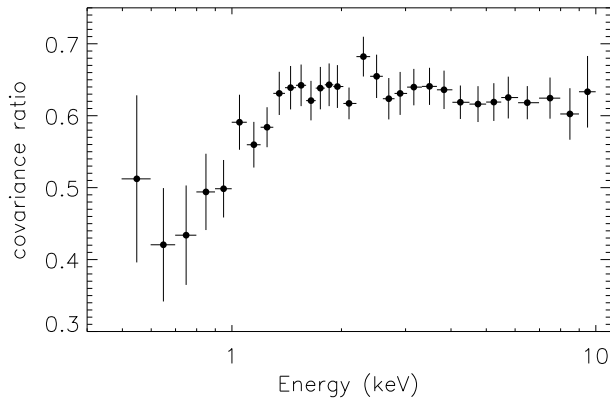


Figure 6. Covariance ratio, derived by dividing the long timescale covariance spectrum by the short timescale one.

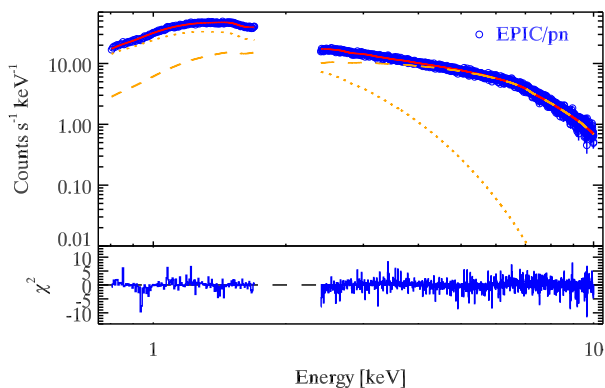


Figure 7. Energy spectrum of the *XMM-Newton* observation based on EPIC/pn data in the range of 0.8 – 10 keV, ignoring energies between 1.7 and 2.4 keV. Data points, best fit model (model B; see Table 2) and individual model components are given (disc blackbody: dotted line; Comptonization component: dashed line).

3.2 *XMM-Newton* data

3.2.1 Timing properties

The soft band PDS (1 – 2 keV) can be well fitted by one zero centered Lorentzian describing the BLN component, one peaked Lorentzian for the QPO at 0.192 ± 0.002 Hz and two peaked Lorentzians for two noise components that peak at $0.11^{+0.02}_{-0.01}$ and $0.47^{+0.02}_{-0.03}$ Hz (Fig. 4). The broadband PDS (2 – 10 keV) can be fitted with the same components (see Table 1). To study the energy dependence of the rms amplitude and of the characteristic frequency we fit PDS obtained in energy bands with a width of 2 keV, namely: 1 – 3, 3 – 5, 5 – 7, and 7 – 9 keV. The characteristic frequency of the BLN component (red crosses in upper panel of Fig. 5) shows a slight increase with increasing energy. This energy dependence of the characteristic frequency has already been observed during LHS observations of other BHBs (Stiele & Yu 2015).

We also derive covariance ratios by dividing the long timescale covariance spectrum by the short timescale one. The covariance spectra are derived following Wilkinson & Uttley (2009) and Stiele & Yu (2015). Taking a look at the PDS (Fig. 4) we use bins of 8 times the frame time measured in segments of 30 bins for the short timescale range and bins of 646 times the frame time

measured in segments of 70 bins for the long timescale range. With this selection we compare variability measured in the flat part of the PDS to the one measured in the decaying part, excluding contribution from the QPO. The obtained covariance ratios are shown in Fig. 6. At energies above 1 keV the covariance ratios are flat, while at lower energies the covariance ratio decreases with decreasing energy. This behaviour clearly differs from the increase of the covariance ratio towards lower energies, which has been found in later phases of the LHS in GX 339-4 and Swift J1753.5-0125 and has been interpreted as the sign of additional disc variability on longer timescales (Wilkinson & Uttley 2009). It is more consistent with the flat covariance ratio observed in the 2008 and 2014 outbursts of H 1743-322 (Stiele & Yu 2016).

3.2.2 Spectral properties

We fit the averaged EPIC/pn spectrum within *isis* V. 1.6.2 (Houck & Denicola 2000) in the 0.8 – 10 keV range, grouping the data to ensure that we have at least 20 source counts in each bin. We exclude the energy range between 1.7 and 2.4 keV from the EPIC/pn spectrum, as this energy range is affected by features caused by gain shift due to Charge-transfer inefficiency around 1.8 and 2.2 keV. We include a systematic uncertainty of 1 per cent. Using an absorbed power law model, as we did for the *Swift* data, and including an additional Gaussian component to model the excess emission below 1.3 keV (Hiemstra et al. 2011; Díaz Trigo et al. 2014), we obtain a foreground absorption of $8.36^{+0.05}_{-0.04} \times 10^{21}$ cm⁻² and a photon index of $1.577^{+0.004}_{-0.003}$, which are lower than the values obtained from the *Swift* observation taken on the same day ($n_{\text{H}} = 10.17 \pm 0.26 \times 10^{21}$ cm⁻²; $\Gamma = 1.612 \pm 0.023$). With a reduced χ^2 of 2219.0/1701 the fit is unacceptable, indicating that additional components are needed to describe the EPIC/pn spectrum properly.

Using an absorbed (tbabs) disc blackbody (diskbb; Mitsuda et al. 1984) plus a thermal Comptonisation component (nthcomp; Zdziarski et al. 1996; Życki et al. 1999) including reflection (reflect; Magdziarz & Zdziarski 1995) we got an acceptable fit with $\chi^2_{\text{red}} = 1682.1/1697$ (Fig. 7). The individual spectral parameters are given in Table 2. Including a disc blackbody and reflection, the photon index gets even lower ($\Gamma = 1.44^{+0.06}_{-0.05}$). The obtained inner disc temperature of $0.62^{+0.03}_{-0.04}$ keV is lower than what has been observed with RXTE for a hard state ($kT_{\text{in}} \sim 0.8 - 0.9$ keV; see e. g. Motta et al. 2010, 2011; Muñoz-Darias et al. 2011). The inner disc radius is at least $55.6^{+5.2}_{-3.6}$ km/ $\sqrt{\cos(\theta)}$ (assuming a distance of more than 25 kpc), which is bigger than what has been observed with RXTE in other BHBs ($R_{\text{in}} \sim 40$ km; see e. g. Motta et al. 2010, 2011; Muñoz-Darias et al. 2011). This can be related to the fact that RXTE allowed only to get energy spectra above 3 keV, in the energy range that is dominated by non-thermal emission in the LHS, and therefore no disc component was needed to fit these spectra.

To compare the energy spectrum to those obtained in Stiele & Yu (2015) we also fit the model used in this paper, which includes a high-energy cutoff component (higcut) instead of a reflection component. We got an acceptable fit with $\chi^2_{\text{red}} = 1638.4/1696$. The photon index ($\Gamma = 1.51^{+0.05}_{-0.03}$) and inner disc radius ($R_{\text{in}} = 55.1^{+5.6}_{-3.7}$ km/ $\sqrt{\cos(\theta)}$) are in agreement with the values obtained with the model including a reflection component, while the inner disc temperature ($T_{\text{in}} = 0.50^{+0.01}_{-0.02}$ keV) is slightly lower.

In addition, we substitute the reflected non-thermal component by the relativistic reflection model `relxill` (Dauser et al. 2014; García et al. 2014) and obtain a fit with $\chi^2_{\text{red}} = 1595.7/1695$. With this model we obtain a photon index of 1.52 ± 0.01 , an inner disc temperature of 0.33 ± 0.02 keV, and an inner disc radius of

$105.3^{+19.4}_{-30.5}$ km/ $\sqrt{\cos(\theta)}$. The *relxill* model gives a spin between -0.930 and -0.998 .

4 DISCUSSION

We used *Swift*/XRT and *XMM-Newton*/EPIC pn data to study the 2015 outburst of GS 1354–64. The spectra obtained from the *Swift* monitoring data can be fitted with a power law model with a photon index in the range of 1.3 – 1.6. This indicates that the source stays in the hard state during the entire outburst. This result is confirmed by the timing properties.

Before the 2015 outburst GS 1354–64 showed an outburst in 1997 during which it also stayed in the LHS during the entire outburst (Revnivtsev et al. 2000; Brocksopp et al. 2001). During the 1997 outburst a similar photon index was observed ($\Gamma = 1.4 - 1.5$; Revnivtsev et al. 2000). There are three even earlier detections of X-ray activity of transient sources that can be spatially related to GS 1354–64. During two of these detections the source was in the HSS, while the remaining one caught a source in the LHS (see Tanaka & Lewin 1995, and references therein). In case all observations are related to the same source this source shows “normal” outbursts with LHS and HSS and so-called “failed” outbursts where it stays in the LHS during the entire outburst. A BHB that is known to show both types of outbursts is H 1743-322 (Stiele & Yu 2016, and references therein). Unlike GS 1354–64 H 1743-322 shows outbursts quite frequently. Another possibility is that only the “failed” outbursts are related with GS 1354–64 and that the HSS are from a nearby transient source. About ten X-ray binaries (including neutron stars and black holes) are known that have only been observed during outbursts where they stayed in the LHS (Capitanio et al. 2009, and references therein). To be certain that GS 1354–64 belongs to the type of BHBs that show “normal” outbursts we would need to observe a HSS with a modern X-ray satellite that allows to confirm that the thermal X-ray emission is spatially consistent with the position of GS 1354–64 obtained during the observation of the Comptonized emission during the 2015 outburst.

The covariance ratio obtained from the *XMM-Newton* observation decreases with decreasing energy below 1 keV, while the one obtained for LHS observations of GX 339–4 and Swift J1753.5–0125 increases with decreasing energy (Wilkinson & Uttley 2009; Stiele & Yu 2015). The increase of the covariance ratio towards lower energies has been interpreted as a sign of additional disc variability on longer timescales. Thus the decrease observed in GS 1354–64 can be either regarded as a sign of missing disc variability on longer timescales or as a sign of additional variability on short timescales. For two observations of H 1743-322 taken during the 2008 and 2014 “failed” outbursts we also found covariance ratios that do not show an increase at lower energies. In case of H 1743-322 the covariance ratios remained rather flat (Stiele & Yu 2016).

In Stiele & Yu (2015) we investigated the energy dependence of the characteristic frequency of the band-limited noise in PDS and found that for a noise component with a characteristic frequency above 1 Hz the characteristic frequency in the 1 – 2 keV band is lower than in the 4 – 8 keV. From the *XMM-Newton* data of GS 1354–64 we obtain a characteristic frequency of $2.85^{+0.85}_{-0.66}$ Hz in the 1 – 2 keV band which is lower than the characteristic frequency of $4.64^{+1.53}_{-1.14}$ Hz in the 4 – 8 keV band, although this result is not significant as the errors are big. The sources investigated in Stiele & Yu (2015) showed either an increase of the covariance ratio towards lower energies or the covariance ratio was flat. The fact

that we observe the same energy dependence of the characteristic frequency as in Stiele & Yu (2015) while the energy dependence of the covariance ratio at soft energies is inverted gives additional evidence that there is no connection between the energy dependence of the characteristic frequency and the covariance ratio. In the cases of H 1743-322 where we found flat covariance ratios there is no energy dependence of the characteristic frequency (Stiele & Yu 2015, 2016).

Fitting the energy spectrum with the same model that has been used in Stiele & Yu (2015), we found that the energy spectrum of GS 1354–64 differed significantly from those studied in Stiele & Yu (2015). The inner disc temperature of GS 1354–64 is significantly higher than the temperatures found in the previous study, while the disc blackbody normalisation, photon index, and cut-off and fold energies are lower. With a higher inner disc temperature and a smaller inner disc radius the observed covariance ratio cannot be explained by a faint disc component and it is more likely that the differences in covariance ratio are related to some changes in the accretion process. We note that all three observations that do not show increasing covariance ratio towards lower energies have energy spectra that require a rather low photon index and were taken during “failed” outbursts. Therefore different shapes of covariance ratio, although observed at soft energies, might be driven by changes in the Comptonizing component or they indicate changes in the accretion geometry that determine if a BHB goes into a “normal” or “failed” outburst. In the case of H 1743-322 the different shape of the covariance ratio can also be related to the higher inclination angle of this source in comparison to the inclination of GX 339–4 or Swift J1753.5-0125 (Stiele & Yu 2016). For GS 1354–64 the inclination angle is not known.

A further investigation of these different possibilities must be the aim of future studies as more data are needed. Further insight can be obtained by observations of other sources during a “failed” outburst or at high inclination to extend the size of the sample or by an observation of H 1743-322 in an early LHS with *XMM-Newton* during a “normal” outburst.

ACKNOWLEDGMENTS

This project is supported by the Ministry of Science and Technology of the Republic of China (Taiwan) through grants 103-2628-M-007-003-MY3 and 104-281-M-007-060.

References

- Arnaud K. A., 1996, in G. H. Jacoby & J. Barnes ed., *Astronomical Data Analysis Software and Systems V* Vol. 101 of *Astronomical Society of the Pacific Conference Series*, XSPEC: The First Ten Years. p. 17
- Belloni T., Hasinger G., 1990, *A&A*, 227, L33
- Belloni T., Parolin I., Del Santo M., Homan J., Casella P., Fender R. P., Lewin W. H. G., Méndez M., Miller J. M., van der Klis M., 2006, *MNRAS*, 367, 1113
- Belloni T., Psaltis D., van der Klis M., 2002, *ApJ*, 572, 392
- Brocksopp C., Bandyopadhyay R. M., Fender R. P., 2004, *New Astron.*, 9, 249
- Brocksopp C., Jonker P. G., Fender R. P., Groot P. J., van der Klis M., Tingay S. J., 2001, *MNRAS*, 323, 517
- Capitanio F., Belloni T., Del Santo M., Ubertini P., 2009, *MNRAS*, 398, 1194

- Casares J., Orosz J. A., Zurita C., Shahbaz T., Corral-Santana J. M., McClintock J. E., Garcia M. R., Martínez-Pais I. G., Charles P. A., Fender R. P., Remillard R. A., 2009, *ApJS*, 181, 238
- Casella P., Belloni T., Stella L., 2005, *ApJ*, 629, 403
- Dauser T., García J., Parker M. L., Fabian A. C., Wilms J., 2014, *MNRAS*, 444, L100
- Del Santo M., Belloni T. M., Tomsick J. A., Sbarufatti B., Cadolle Bel M., Casella P., Castro-Tirado A., Corbel S., Grinberg V., Homan J., Kalemci E., Motta S., Muñoz-Darias T., Pottschmidt K., Rodríguez J., Wilms J., 2015, *ArXiv e-prints*
- Díaz Trigo M., Migliari S., Miller-Jones J. C. A., Guainazzi M., 2014, *A&A*, 571, A76
- Francey R. J., 1971, *Nature Physical Science*, 229, 229
- García J., Dauser T., Lohfink A., Kallman T. R., Steiner J. F., McClintock J. E., Brenneman L., Wilms J., Eikmann W., Reynolds C. S., Tombesi F., 2014, *ApJ*, 782, 76
- Hiemstra B., Méndez M., Done C., Díaz Trigo M., Altamirano D., Casella P., 2011, *MNRAS*, 411, 137
- Houck J. C., Denicola L. A., 2000, in N. Manset, C. Veillet, & D. Crabtree ed., *Astronomical Data Analysis Software and Systems IX Vol. 216 of Astronomical Society of the Pacific Conference Series, ISIS: An Interactive Spectral Interpretation System for High Resolution X-Ray Spectroscopy*. p. 591
- Leahy D. A., Elsner R. F., Weisskopf M. C., 1983, *ApJ*, 272, 256
- Magdziarz P., Zdziarski A. A., 1995, *MNRAS*, 273, 837
- Makino F., 1987, *IAU Circ.*, 4342, 1
- Markert T. H., Laird F. N., Clark G. W., Hearn D. R., Sprott G. F., Li F. K., Bradt H. V., Lewin W. H. G., Schnopper H. W., Winkler P. F., 1979, *ApJS*, 39, 573
- Miller J. M., Reynolds M. T., Kennea J., 2015, *The Astronomer's Telegram*, 7612
- Mitsuda K., Inoue H., Koyama K., Makishima K., Matsuoka M., Ogawara Y., Suzuki K., Tanaka Y., Shibasaki N., Hirano T., 1984, *PASJ*, 36, 741
- Motta S., Muñoz-Darias T., Belloni T., 2010, *MNRAS*, 408, 1796
- Motta S., Muñoz-Darias T., Casella P., Belloni T., Homan J., 2011, *MNRAS*, 418, 2292
- Muñoz-Darias T., Motta S., Belloni T. M., 2011, *MNRAS*, 410, 679
- Muñoz-Darias T., Motta S., Stiele H., Belloni T. M., 2011, *MNRAS*, 415, 292
- Revnivtsev M. G., Borozdin K. N., Priedhorsky W. C., Vikhlinin A., 2000, *ApJ*, 530, 955
- Rodríguez J., Shaw S. E., Corbel S., 2006, *A&A*, 451, 1045
- Stiele H., Yu W., 2015, *MNRAS*, 452, 3666
- Stiele H., Yu W., 2016, *ArXiv:1602.01550*
- Sturner S. J., Shrader C. R., 2005, *ApJ*, 625, 923
- Swinbanks D., 1987, *Nature*, 326, 322
- Tanaka Y., Lewin W. H. G., 1995, *X-ray Binaries*, pp 126–174
- Verner D. A., Ferland G. J., Korista K. T., Yakovlev D. G., 1996, *ApJ*, 465, 487
- Wijnands R., Homan J., van der Klis M., 1999, *ApJ*, 526, L33
- Wilkinson T., Uttley P., 2009, *MNRAS*, 397, 666
- Wilms J., Allen A., McCray R., 2000, *ApJ*, 542, 914
- Zdziarski A. A., Johnson W. N., Magdziarz P., 1996, *MNRAS*, 283, 193
- Zhang W., Jahoda K., Swank J. H., Morgan E. H., Giles A. B., 1995, *ApJ*, 449, 930
- Życki P. T., Done C., Smith D. A., 1999, *MNRAS*, 309, 561

Table 3. Spectral parameters obtained by fitting the *Swift*/XRT spectra.
(cont.)

| obs [†] | time* | χ^2_{red} | $n_H^{\#}$ | Γ | norm ⁺ | flux $_{\text{abs}}^{\ddagger}$ | flux $_{\text{unabs}}^{\ddagger}$ | $\chi^2_{\text{red}}^{\blacklozenge}$ | Γ^{\blacklozenge} | norm ^{+,\blacklozenge} | flux $_{\text{abs}}^{\ddagger,\blacklozenge}$ | flux $_{\text{unabs}}^{\ddagger,\blacklozenge}$ |
|------------------|-------|-----------------------|--------------------------------------|--|---|---------------------------------|-----------------------------------|---------------------------------------|--|--|---|---|
| 52 | 88.2 | 0.88 | 8.7 ^{+0.7} _{-0.6} | 1.54 ^{+0.06} _{-0.06} | 0.092 ^{+0.008} _{-0.007} | 5.33 | 6.91 | 0.88 | 1.53 ^{+0.04} _{-0.04} | 0.090 ^{+0.003} _{-0.003} | 5.34 | 6.89 |
| 53 | 90.6 | 0.99 | 8.6 ^{+0.8} _{-0.8} | 1.51 ^{+0.07} _{-0.07} | 0.081 ^{+0.008} _{-0.007} | 4.91 | 6.30 | 0.99 | 1.51 ^{+0.04} _{-0.04} | 0.081 ^{+0.004} _{-0.003} | 4.91 | 6.30 |
| 54 | 92.5 | 0.93 | 10.1 ^{+1.0} _{-0.9} | 1.59 ^{+0.08} _{-0.08} | 0.076 ^{+0.008} _{-0.007} | 4.01 | 5.40 | 0.96 | 1.47 ^{+0.04} _{-0.04} | 0.065 ^{+0.003} _{-0.003} | 4.13 | 5.24 |
| 55 | 94.3 | 1.03 | 9.0 ^{+0.9} _{-0.9} | 1.47 ^{+0.08} _{-0.08} | 0.059 ^{+0.007} _{-0.006} | 3.75 | 4.78 | 1.03 | 1.44 ^{+0.05} _{-0.05} | 0.056 ^{+0.003} _{-0.003} | 3.78 | 4.75 |
| 57 | 98.3 | 0.94 | 9.5 ^{+3.1} _{-2.5} | 1.51 ^{+0.27} _{-0.24} | 0.046 ^{+0.018} _{-0.012} | 2.76 | 3.59 | 0.91 | 1.44 ^{+0.14} _{-0.14} | 0.042 ^{+0.006} _{-0.006} | 2.81 | 3.54 |
| 58 | 100.0 | 1.09 | 10.3 ^{+1.3} _{-1.2} | 1.49 ^{+0.11} _{-0.10} | 0.045 ^{+0.007} _{-0.006} | 2.73 | 3.57 | 1.12 | 1.37 ^{+0.05} _{-0.05} | 0.038 ^{+0.002} _{-0.002} | 2.82 | 3.47 |
| 59 | 102.4 | 1.23 | 9.6 ^{+1.3} _{-1.2} | 1.41 ^{+0.11} _{-0.11} | 0.035 ^{+0.006} _{-0.005} | 2.44 | 3.09 | 1.23 | 1.34 ^{+0.06} _{-0.06} | 0.032 ^{+0.002} _{-0.002} | 2.49 | 3.05 |
| 60 | 104.0 | 1.23 | 11.9 ^{+1.4} _{-1.3} | 1.57 ^{+0.11} _{-0.11} | 0.043 ^{+0.007} _{-0.006} | 2.26 | 3.10 | 1.36 | 1.34 ^{+0.05} _{-0.05} | 0.031 ^{+0.002} _{-0.002} | 2.39 | 2.92 |
| 61 | 106.4 | 1.10 | 8.7 ^{+1.4} _{-1.3} | 1.35 ^{+0.12} _{-0.12} | 0.026 ^{+0.005} _{-0.004} | 2.00 | 2.45 | 1.09 | 1.35 ^{+0.07} _{-0.07} | 0.026 ^{+0.002} _{-0.002} | 2.00 | 2.45 |
| 62 | 108.2 | 0.94 | 8.8 ^{+1.6} _{-1.4} | 1.40 ^{+0.13} _{-0.12} | 0.024 ^{+0.004} _{-0.004} | 1.71 | 2.13 | 0.93 | 1.39 ^{+0.07} _{-0.07} | 0.024 ^{+0.002} _{-0.002} | 1.71 | 2.13 |
| 63 | 110.8 | 0.87 | 11.4 ^{+1.6} _{-1.5} | 1.51 ^{+0.13} _{-0.12} | 0.028 ^{+0.005} _{-0.004} | 1.66 | 2.21 | 0.95 | 1.32 ^{+0.06} _{-0.06} | 0.021 ^{+0.001} _{-0.001} | 1.74 | 2.12 |
| 65 | 114.7 | 1.37 | 13.6 ^{+4.3} _{-3.7} | 1.70 ^{+0.31} _{-0.29} | 0.037 ^{+0.018} _{-0.012} | 1.58 | 2.32 | 1.47 | 1.35 ^{+0.13} _{-0.13} | 0.023 ^{+0.003} _{-0.003} | 1.73 | 2.12 |

Notes: *: days since June 10th 2015 00:00:00.000 UTC

[†]: *Swift* obs id: 000338110xx

[‡]: 10^{-10} erg cm⁻² s⁻¹

⁺: photons keV⁻¹ cm⁻² s⁻¹ at 1 keV

[#]: 10^{21} cm⁻²

[•]: n_H fixed at the average of 8.6×10^{21} cm⁻²

Table 4. Parameters of the PDS of *Swift* observations that show type-C QPOs

| obs [†] | BLN | | ν [Hz] | QPO | | harmonic/ add. comp. | | |
|------------------|---------------------------|----------------------|---------------------------|---------------------------|----------------------|---------------------------|---------------------------|---------------------|
| | Δ [Hz] | rms [%] | | Δ [Hz] | rms [%] | ν [Hz] | Δ [Hz] | rms [%] |
| 37 | $0.702^{+0.167}_{-0.124}$ | $18.7^{+1.3}_{-1.5}$ | $0.183^{+0.005}_{-0.004}$ | $0.007^{+0.004}_{-0.003}$ | $8.9^{+1.4}_{-1.5}$ | 0 | $0.028^{+0.012}_{-0.010}$ | $9.7^{+1.4}_{-1.7}$ |
| 38 | $0.154^{+0.044}_{-0.041}$ | $18.3^{+2.4}_{-2.3}$ | $0.182^{+0.009}_{-0.012}$ | $0.015^{+0.015}_{-0.013}$ | $9.1^{+2.1}_{-2.5}$ | $0.420^{+0.020}_{-0.019}$ | $0.039^{+0.026}_{-0.018}$ | $8.2^{+1.8}_{-2.0}$ |
| 39 | $0.258^{+0.053}_{-0.046}$ | $21.5^{+1.3}_{-1.5}$ | $0.215^{+0.010}_{-0.013}$ | $0.018^{+0.008}_{-0.007}$ | $10.3^{+1.8}_{-1.9}$ | | | |
| 41 | $0.325^{+0.042}_{-0.034}$ | 23.3 ± 0.9 | $0.192^{+0.005}_{-0.006}$ | $0.021^{+0.007}_{-0.006}$ | $11.2^{+1.3}_{-1.4}$ | $0.399^{+0.002}_{-0.001}$ | < 0.004 | $4.4^{+0.7}_{-0.9}$ |
| 42 | $0.454^{+0.175}_{-0.098}$ | $19.1^{+1.5}_{-1.8}$ | 0.187 ± 0.010 | $0.020^{+0.009}_{-0.007}$ | 11.9 ± 2.0 | | | |
| 44 | $0.926^{+0.262}_{-0.239}$ | $19.1^{+1.7}_{-1.6}$ | 0.194 ± 0.007 | $0.018^{+0.007}_{-0.008}$ | $11.2^{+1.2}_{-1.5}$ | $0.087^{+0.004}_{-0.005}$ | $0.008^{+0.005}_{-0.004}$ | $7.6^{+1.2}_{-1.4}$ |
| 47 | $3.186^{+3.139}_{-1.787}$ | $29.1^{+4.4}_{-4.9}$ | $0.176^{+0.006}_{-0.005}$ | $0.010^{+0.021}_{-0.010}$ | $10.2^{+2.4}_{-4.2}$ | 0.070 ± 0.030 | $0.040^{+0.181}_{-0.025}$ | > 9.5 |

Notes:

†: *Swift* obs id: 000338110xx

This paper has been typeset from a \TeX / \LaTeX file prepared by the author.